

---

# AERODYNAMIC SHAPE OPTIMIZATION STUDIES OF THE ADODG BENCHMARK PROBLEMS

Shlomy Shitrit<sup>1</sup>

*RAFAEL, Advanced Defense Systems, Ltd., Haifa 31021, Israel*

The following study presents single and multipoint aerodynamic shape optimizations of two benchmark problems defined by the Aerodynamic Design Discussion Group (ADODG). Mesh warping and geometry parametrization is accomplished by fitting the multi-block structured grid to a B-spline volumes and performing the mesh movements by using surface control points embedded with free-form deformation (FFD) volumes. The aerodynamic model solves the RANS equations with Spallart-Almaras turbulence model. A gradient based optimization algorithm is used with an adjoint method in order to compute the objectives and constraints derivatives with respect to the design variables. The objective in this work is to minimize the drag of airfoil and wings for transonic regimes taking into account volume and thickness constraint, including aerodynamic coefficients constraint.

The first problem solved is RAE2822 airfoil in viscous transonic flow, with a lift constraint. The shock in the upper surface is eliminated and the drag coefficient is reduced by 50%. Also in this problem we started the optimization solution from a circle in order to check the robustness of both the flow solver and the mesh warping algorithm, while reaching a "close" solution as obtained by starting from rae2822 airfoil. The second problem is single and multi-point lift and pitch moment constrained drag minimization of the Common Research Model (CRM) wing in transonic, viscous flow. The CRM design is very challenging due to the tight coupling between aerodynamic performance, trim and stability. Other design challenges include the number of design variables and its effect on the optimized configuration. The single-point optimization reduced the drag coefficient by 7.7% using 192 design variables. The single-point designs are relatively robust to the flight conditions. Further robustness is achieved through a multi-point optimization with nearly 5% drag reduction.

## Nomenclature

$M$	=	Mach number
$\alpha$	=	angle of attack, deg
$\rho$	=	density, kg/m <sup>3</sup>
$u, v, w$	=	velocity components, m/s
$p$	=	static pressure, Pa; order of convergence
$E$	=	energy, J
$R$	=	residual
$Re_y$	=	Reynolds number
$FFD$	=	free form deformation
$y^+$	=	yplus
$C_l$	=	lift coefficient
$C_d$	=	drag coefficient
$C_{mz}$	=	pitch moment coefficient
$t$	=	thickness, m
$V$	=	volume, m <sup>3</sup>
$c$	=	chord length, m

---

<sup>1</sup> Research Engineer, CFD group, Aeronautical Systems, P.O. Box 2250; shlomy.shitrit@gmail.com

$GCI$  = grid convergence index  
 $N$  = mesh size  
 $LE$  = leading edge  
 $TE$  = trailing edge  
 $CRM$  = common research model  
 $S$  = area,  $m^2$   
 $L$  = grid level

*Subscripts*

*baseline* = initial configuration  
*ref* = reference value

## I. Introduction

The aerodynamic shape optimization, even for only a wing design, more than ten years ago has been a very difficult task. A typical aerodynamic optimization process requires a robust mesh warping method, grid parametrization, CFD solver and optimization algorithm. The tremendous improvements in each of these fields in the last few years, and the fact that researches made them available as an open source tools, allow aerodynamicists in academy as well as in industry actually perform an aerodynamic shape optimization, and robustly exploring a design space that perfectly fits the engineering requirements. These useful tools allow not only for improving existing designs, but also reach unconventional configurations with much improved performances.

Numerical optimization approaches are usually categorized to gradient-based method and gradient-free methods. The adjoint method for computing the gradients along with an optimizer that is the gradient-based is proven to be the most efficient method for large scale problems with hundreds of design variables [1] [2] [3]. Pironneau [4] first introduced the adjoint method for drag minimization problems, and then Jameson [5] extended to the aerodynamic optimization of the Euler flow in the late 1980's. Since then various researchers have applied this method within complex implementations for aerodynamic problems [6] [7] [8] [9] [10] [11].

One of the popular sensitivity analysis methods is finite differencing, but disadvantages are its high computational cost and low accuracy. Mader et al. [12] presented an automatic differentiation tool and applied it selectively to produce code that computes the flux Jacobian matrix and the other partial derivatives that are necessary for the adjoint method.

The AIAA Aerodynamic Design Optimization Discussion Group (ADODG) proposed a series of benchmark cases, a great initiative that allow researchers around the world to run, compare and make a special thorough analysis of getting the best optimal shapes. The meshes and configurations of the benchmarks are publicly available, and this allows direct comparisons with other solvers.

Since the ADODG useful initiative many publications regarding benchmarks problems are available and among the research studies, the multidisciplinary design optimization (MDO) tools are the most remarkable. Martines et al are involved in a variety of applications, including the optimization of a supercritical airfoil and starting from a circle [13], aircraft aerodynamic [14] and aero structural optimization [15], and aero propulsive optimization. Recently Zhoujie et al. [16] solved a series of aerodynamic shape optimization problem based on the CRM wing. The model solves RANS equations with Spallart-Allamaras turbulence model. A gradient based optimization algorithm is used in conjunction with an adjoint method. The drag coefficient is minimized by 8.5% with respect to lift and pitch moment constrains while using 720 shape

variables. Another issues such as multi-point, no thickness reduction and starting from random geometry are presented and discussed.

Aerodynamic design optimization process is very sensitive to the starting design sometimes and requires trial and error to get a converged optimal design. Xialong et al. [13] addresses this need by developing ways to overcome robustness issues arising from mesh warping, shape parametrization and CFD solver. They demonstrated the NACA0012 and RAE-2822 airfoil benchmarks to show the dominant factors influence the convergence efficiency. In addition they solved a challenging aerodynamic shape optimization case that starts from a circle in order to test the framework robustness. Another experience with this challenge is demonstrated in the present paper, inspired by Xialong et al [13].

A thorough analysis regarding the ADODG benchmark cases is demonstrated by Christopher et al. [17] while using the Jetstream optimization code algorithm. For the NACA 0012 optimization the drag coefficient is reduced by 42 counts and the shock is weakened. For RAE-2822, successful optimizations eliminate the shock, reducing drag coefficient to 119 counts in the best case. In the CRM wing cases, significant shape changes and performance improvements are reported.

Zouhlo et al. [16] presented a series of RANS-based aerodynamic shape optimization of a blended wing body configuration to understand the tradeoffs between the trim, stability and bending moment and the aerodynamic performance. Single-point designs as well as robust multi-point optimization are demonstrated.

The 4<sup>th</sup> Drag Prediction Workshop (DPW-4) CRM wing-body-tail configuration was chosen by Song Chen et al. [14] as the baseline model. Series of wing-body-tail optimizations minimized the drag coefficient subject to lift, pitching moment and geometric constraints. The single-point trim constrained optimization achieved a reduction of 4.1% of the total drag of the trimmed baseline. They found that considering the trim during optimization is a better approach than using a fixed wing moment constraint, and simultaneous optimization of wing and tail rotation is the best way to obtain an improved performance.

The present paper demonstrates a modest experience and first steps done towards the construction of an aerodynamic shape optimization capability while applying the Adflow algorithm which is part of the MDO lab framework that made available as an open-source in the last year (2019-2020). In this paper a large set of results are presented for the computational complicated and intensive NASA Common Research model (CRM) wing. This is a lift constrained drag minimization problem. Besides the single-point optimization problem, two additional problems for the same CRM wing that are not part of ADODG benchmark are solved: a case with no thickness constraints and multi-point optimization.

The tools that are used for this study are a subset of the multidisciplinary design optimization (MDO) framework of aerodynamic configurations (MACH) [18]. With this software one can perform aero-structural optimization, but in the present study only the MACH's components relevant for aerodynamic shape optimization are used: CFD solver, mesh warping, geometric parametrization and optimization algorithm. The availability of these open-source tools and benchmarks enabled further studies in CFD-based aerodynamic design optimization.

This paper is organized as follows. The introduction of the optimization tools are briefly described in Section 2. Sections 3 and 4 describe the optimization results of the RAE-2822 and CRM wing.

## II. Methodology

The drag minimization of the problems presented in this work is obtained by using a CFD solver coupled with an adjoint solver to compute the objectives and constraints sensitivities, a robust

mesh warping routine and a gradient based optimizer. These tools are part of the MACH framework proven to be a useful tool for aerodynamic structural optimization. The pyGeo routine used for geometric manipulation, iDWarp for mesh deformation, Adflow as the flow solver and SLSQP as the numerical optimization algorithm.

#### A. CFD solver

The CFD solver used in this research is three dimensional multi-block structured finite volume solver (SUmber). The parallel implicit solver is capable of solving the Euler and Reynolds averaged Navier-Stokes (RANS) equations (steady and unsteady) [19]. The discretization of the governing equations is done by a finite volume approach with a central formulation over structured meshes. The convective terms are computed by the Jameson-Schmidt-Turkel [20] scheme using flux splitting upwind scheme with Van-Albeda limiter. Viscous fluxes are computed to second order accuracy using a central difference approach. The residual smoothing is made by employing an explicit 5th order Runge-Kutta algorithm employing well known steady-state acceleration techniques including local time stepping, implicit residual smoothing and geometric multigrid. For RANS analysis the turbulent equations are solved in coupled fashion using diagonally-dominant alternating direction implicit (DD-ADI) scheme. In order to improve convergence, the solver is also equipped with a diagonalized ADI method for the mean flow equations and Newton-Krylov (NK) solver. The computational coordinates is x, y and z axes, while x in the stream-wise direction, y vertical, and z span-wise. The origin is located at the airfoil (or wing) leading edge.

The steady state mean flow equations discretized using a finite volume cell centered formulation , yielding a set of ordinary differential equations that can be written as follows:  $R(w_{ijk}) = 0$ , where  $w$  is a vector of the mean flow variables:  $w = \{\rho, \rho u, \rho v, \rho w, \rho E\}^T$ , and  $R$  is the residual obtained by evaluating the sum of integral fluxes of the governing equations, to the second order of accuracy.

#### B. Free Form Deformation (FFD) and mesh warping

The geometry parametrization is done by the FFD approach [21]. In this approach the geometry is located inside a B-Spline control volume while the coordinates are mapped to the external surface of the volume by Newton search algorithm. All the geometric modifications are made on the external surfaces of the FFD volume. Any modification of the FFD boundaries indirectly modifies the internal geometry. The main assumption of this approach is a constant topology throughout the optimization process.

After the FFD volumes modify the geometry during the optimization process, the mesh must be warped in order to solve the flow field for the modified geometry. In this work the algebraic mesh perturbation scheme is used, which is developed by Kenway et al. [21].

#### C. Optimization algorithm

In this research work the SLSQP (sequential least square programming) optimization algorithm is applied. It is part of the pyOpt framework Perez [22] which is an open source software. The algorithm SLSQP [23] is evolved from the least squares solver [8]. It uses a quasi-Newton Hessian approximation and an L1-test function in the line search algorithm.

### III. RAE-2822 Airfoil in viscous transonic flow

#### A. Problem formulation

The first optimization problem presented here is the drag coefficient minimization of the ADODG RAE-2822 airfoil viscous transonic flow. Mesh convergence study was performed with three families of meshes. The Mach number  $M = 0.734$  calculated at Reynolds number

$Rey = 6.5M$ . The aerodynamic optimization problem formulation is summarized in Table 1, where  $C_l$  and  $C_m$  are the lift and moment coefficient. The lift coefficient is constrained to  $c_l = 0.824$  and the pitch moment coefficient about the quarter chord must be higher than  $c_{mz} = -0.092$ . The airfoil area must be no less than the initial area. The design space includes 25 control points in chord wise direction, as vertical movement of the FFD control points in y direction. Relative thickness ( $t/c$ ) constraints are enforced at 25 positions along the chord to ensure that the airfoil thickness is larger or equal to that of the baseline.

**Table 1: ADODG RAE-2822 case problem statement**

Objective	Name	Quantity	Lower value, m	Upper value, m
Design variables	Minimum Cd	1	-	-
	y	40	-0.05	0.05
Constraints	$\alpha$	1	1	5
	$C_m$	1	-0.092	-
	$C_l$	1	0.824	0.824
	t/c	400	$10^{-4}$	-

A 3-D airfoil geometry is constructed with a span of 0.1 m in z direction, with two symmetry planes. The O-grid topology includes 31360 (level L1) cells with 246 cells in chord wise direction and 129 cells perpendicular to the airfoil surface. The minimum cell size close to the boundary is  $3 * 10^{-6} m$ , reaching  $y^+ \approx 0.4$  in zero angle of attack. Grid convergence study was conducted while refining the grid in chordwise and normal direction, keeping  $y^+ \sim 1$ . The aerodynamic coefficients results of four different grid refinement levels are collected in

Table 2 computed in  $M = 0.734$  and  $\alpha = 2.47^\circ$ .

### B. Grid convergence study

Grid convergence study has been made based on the Grid Convergence Index (GCI) method, for examining the spatial convergence of CFD simulations presented in the book by Roache [24]. Roache suggests a GCI to provide a consistent manner in reporting the results of grid convergence studies and also an error band on the grid convergence of the solution. This approach is also based upon a grid refinement estimator derived from the theory of Richardson Extrapolation [7]. The GCI on the fine grid is defined as:  $GCI_{fine} = \frac{F_s}{r^{p-1}}$  where  $F_s$  is a factor of safety (recommended to be  $F_s = 1.25$  for comparisons over three or more grids). The GCI for coarser grid is defined as:  $GCI_{coarse} = \frac{F_s r^p}{r^{p-1}}$ , while each grid level yield solutions that are in the asymptotic range of convergence for the computed solution. The parameter p is the order of convergence (here a second order accuracy is involved, so theoretically the maximum value is p=2), and r is the effective grid ratio:  $r = \left(\frac{N_1}{N_2}\right)^{1/d}$  where N is the total number of grid points in executive grid levels, and d is the flow dimension. Since the grid was adapted only in two directions (chordwise and normal directions) and in spite of the fact that we actually solve 3D problem, a d=2 is defined. The asymptotic range of convergence can be checked by observing

the two GCI values as computed over three grids,  $GCI_{23} = r^p GCI_{12}$  while values approximately unity indicates that the solutions are within the asymptotic range of convergence.

For this purpose three levels of grid refinement have been checked to assess the effect on the numerical accuracy, while the total grid cells number:  $L0 = (490 \times 257)$  126162 cells,  $L1 = (245 \times 129)$  31360 cells and  $L2 = (123 \times 65)$  7872 cells. The grids generated with clustering cells near the walls which results in a maximum of  $y^+ \approx 0.4$  in all the computed angles of attack.

A polar graph of the drag coefficient is presented in Figure 1. The GCI values including the asymptotic range of convergence and an estimation of the aerodynamic coefficient values at zero grid spacing are detailed in Table 3, computed at  $\alpha = 0^\circ$ . Based on this study we can say, for example, that  $Cd$  is estimated to be  $Cd = 0.0097742$  with an error band of 9.2455%. The grid resolution studies confirmed that the computed aerodynamic coefficients values are grid converged.

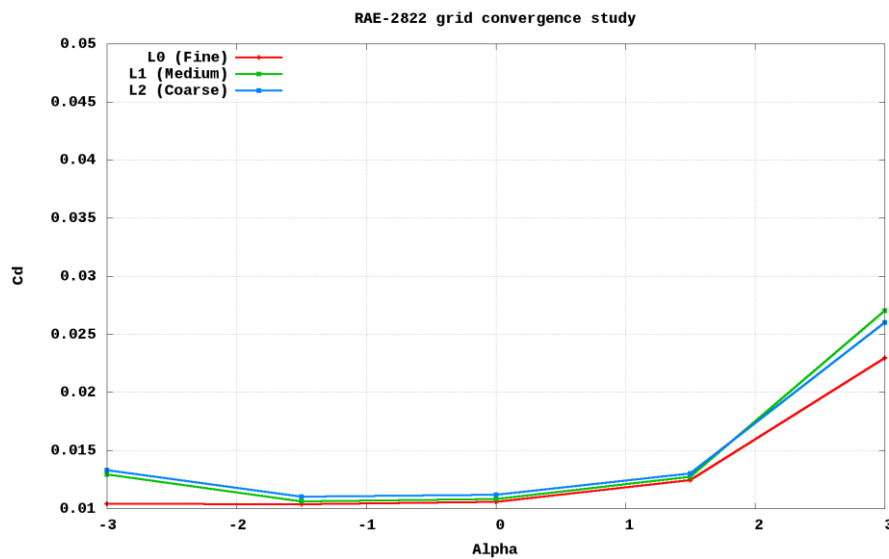


Figure 1: Drag coefficient Vs. angle of attack in grid convergence study

Table 2: Mesh convergence checks for RAE-2822 airfoil at  $M=0.734$ ,  $\alpha = 3^\circ$

Grid level	Cd	Cl	Cmz	Y+	$\alpha$ [deg]
L0, 490X257-126162 cells	0.0223	0.7739	0.0921	0.4	3
L1, 245X129-31360 cells	0.0270	0.8963	0.1114	0.4	3
L2, 123X65-7872 cells	0.0260	0.8642	0.1048	0.4	3

Table 3: Aerodynamic coefficient results of the grid convergence study at  $\alpha = 0^\circ$

	Grid level	Grid ratio, r	GCI [%]	Richardson extrapolation	Asymptotic convergence range
$C_d$	L0	1	-	0.0097742	1.02576
	L1	2.0	9.2455	-	-
	L2	4.0	12.153	-	-
	L0	1	-	0.3444	0.9984

$C_l$	L1	2.0	0.0187	0.0973	1.0057
	L2	4.0	0.2151		
$C_m$	L0	1	-		
	L1	2.0	3.3818		
	L2	4.0	4.0707		

In order to evaluate the grid convergence and accuracy, the numerical results of the pressure coefficient value around the airfoil is compared to experimental results for the RAE-2822 [25]. The flow conditions were changed according to the experiment setup to  $M = 0.73$  and corrected wind tunnel angle of attack  $\alpha = 2.79^\circ$ . The analysis with the finest grid level gives a lift coefficient  $C_l = 0.8746$ , drag coefficient  $C_d = 0.02196$  and pitch moment coefficient  $C_{mz} = 0.10806$ . The experimental results are:  $C_l = 0.803$ ,  $C_d = 0.0168$  and  $C_{mz} = 0.099$ . In Figure 3 the pressure coefficient values distribution are compared.

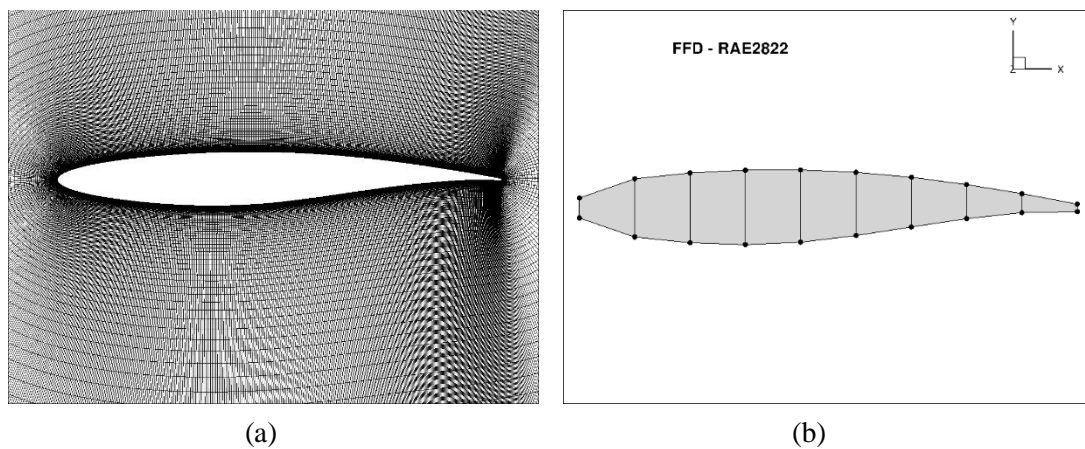


Figure 2: a) Fine grid of RAE-2822 used for optimization. b) The FFD grid includes 40 control points

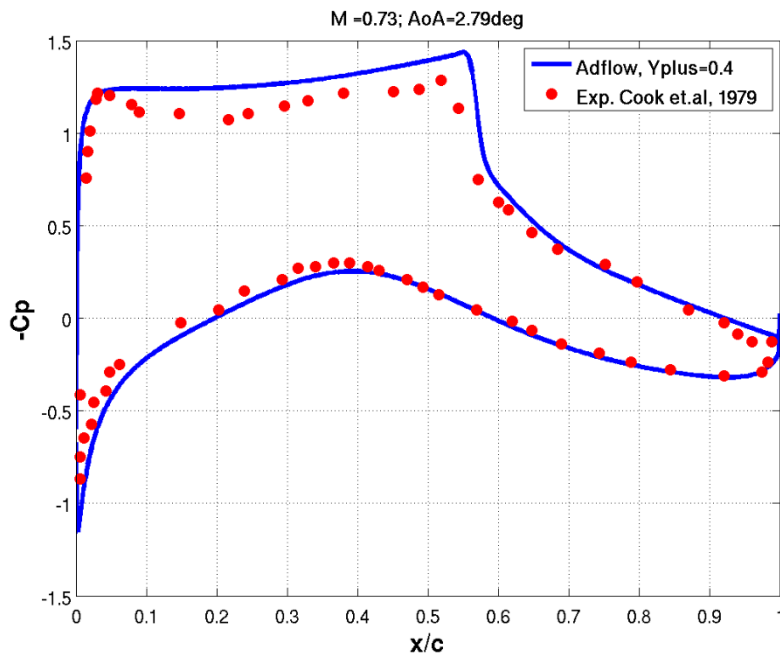


Figure 3: Comparison of computational and experimental pressure coefficient values

### C. Optimization results

The drag, lift and pitch moment coefficients are plotted (see Figure 4) against the optimization iterations number. The drag coefficient reduction of 971 Counts (1 drag count =  $10^{-4}Cd$ ) (49.2%) was obtained. The optimized results were obtained after 100 design iterations and the lift, drag and pitch moment coefficients are compared in Table 4. Figure 5 shows the pressure coefficient distribution (left figure) and the baseline and optimized airfoil shape. It is clearly seen that the shock wave appeared in the baseline configuration is eliminated in the optimized shape. The airfoil's thickness is reduced by nearly 15% compared to the initial value.

The flow converge to a density residual of  $10^{-12}$  and the adjoint equation convergence was set also to  $10^{-12}$ . The optimality convergence tolerance of SLSQP optimization algorithm was set to  $10^{-6}$ . In this case different number of design variables was checked, but increasing the number of control points higher than 40 (20 chordwise stations and 2 symmetry planes) has a negligible effect on the optimal shape and pressure distribution.

In Table 4 the optimized results are compared with those reported by other published results. A possible source to the difference in the results is that the mesh topology and flow solvers used by each paper are different. Another reason that should contribute to different results is the mesh warping and parametrization method.

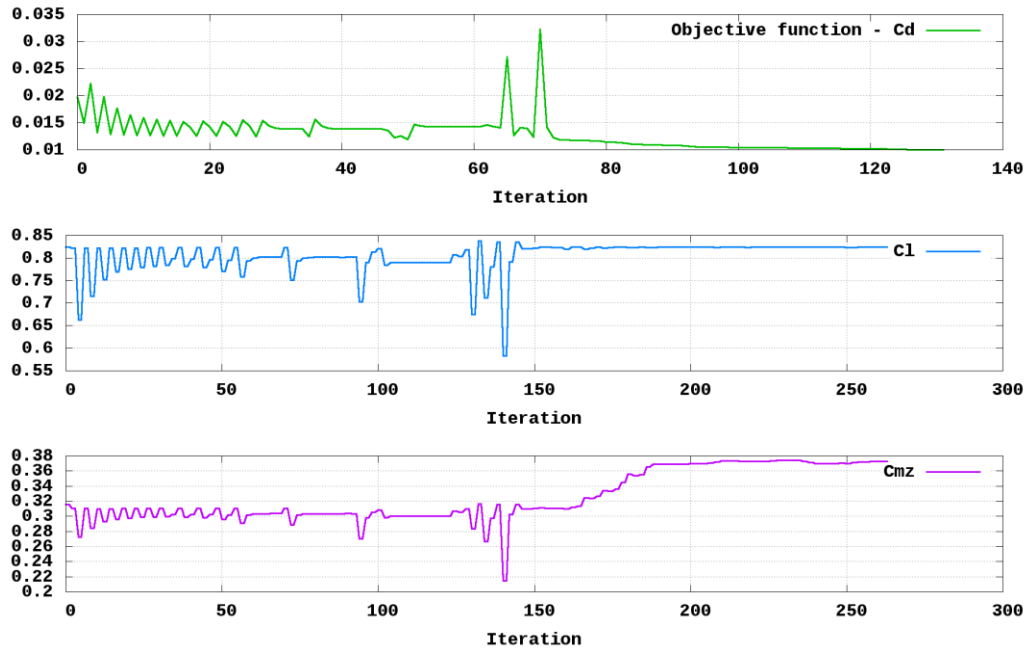


Figure 4: Drag, lift and pitch moment coefficients against the number of iterations

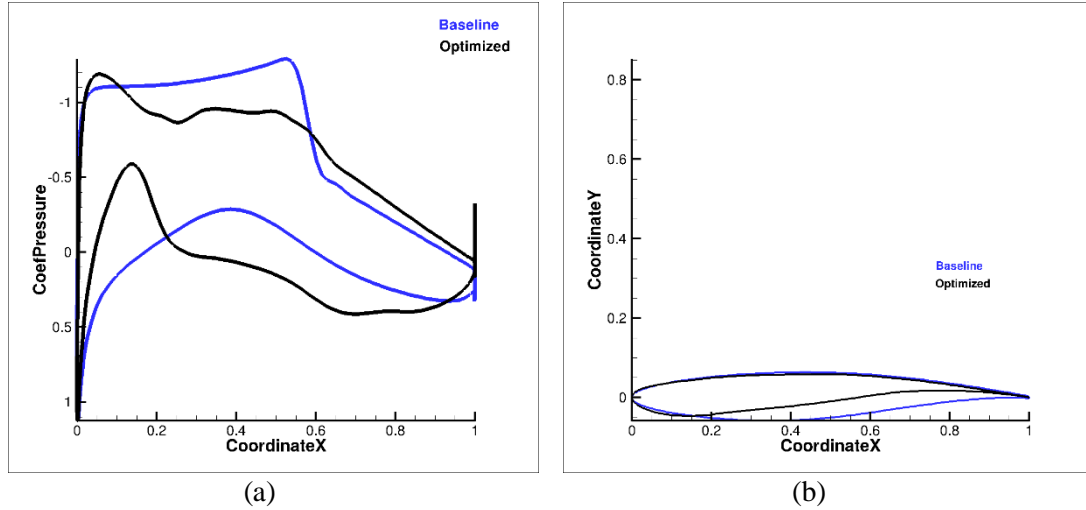


Figure 5: Baseline and optimized results. a) Pressure coefficient distribution. b) A comparison of the airfoil shapes

Table 4: Comparison of optimized results between the present work, Christopher et al. [17] and Xiaolong et al. [13]

Case	AoA [deg]	Cl	Cd (initial)	Cd (Optimized)	Change (Counts)
<b>Present work</b>	2.47	0.8237	0.01970	0.01002	96.8
<b>Christopher et al. [17]</b>	2.817	0.824	0.019841	0.010989	88.5
<b>Xiaolong He et al. [13]</b>	2.817	0.824	0.019841	0.010975	88.6

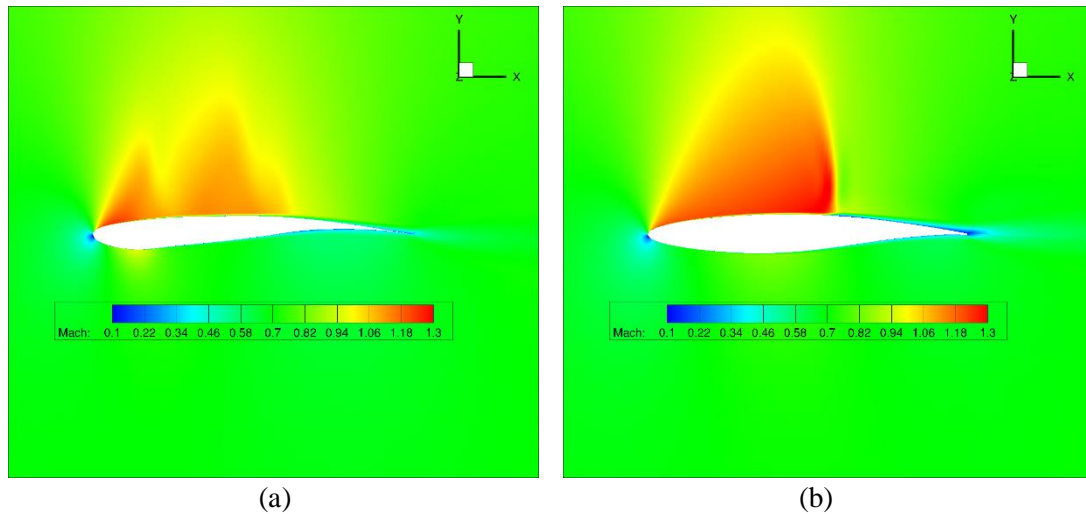


Figure 6: Mach number distribution of the baseline (a) and optimized (b) results

#### D. Optimization starting from a circle

Now a new challenging aerodynamic optimization process is created by starting from a circle, while the previous case started from an airfoil RAE-2822. This is a much bigger challenge that examines effectiveness of the FFD parametrization process as well as the ability of the flow solver to reach convergence. However, besides all these robustness demonstrations, this starting condition has no industrial benefit what so ever. This is no surprise since no one would start from a circle in order to reach an optimized airfoil. The same flow conditions and constraints are used as for the previous case of RAE-2822 case.

For this purpose a structured O-mesh is constructed for the circle geometry by using pyHyp procedure, while the mesh includes 31605 cells (245 cells in the spatial direction and 129 in the normal direction). The farfield is located 100C.

First the transonic problem is solved by using a single unmodified FFD frame that includes total of 20 control points (10 points in chordwise direction in top and lower circle parts, separately, and total of 40 control points). But, in this approach an anomalous shapes encountered during the optimization process, besides the difficulties to reach convergence since IDWarp fails due to negative volumes cells. One way to handle this problem (which finally did not accomplished) is to generate the mesh for the modified geometry by using pyHyp, but since all the optimization process already took more than 200 iterations, this approach is finally abandoned.

The second approach includes a modified FFD parametrization. In this way the optimization problem is decomposed to three stages which differs one form the other in the FFD resolution. In the first stage the FFD frame includes 3 control points (total of 12) in chordwise direction. Three control points accomplish a large thickness reduction in four iterations only. The first stage includes a total of 16 iterations for reaching a nice smooth airfoil, while the optimized results including the final shape serve as a starting conditions to the second optimization stage. In the second stage three control points are added to the FFD (total of 24 equally spaced control points) and after 70 more iterations reached convergence. The second stage manages to achieve a supercritical airfoil shape, which again serves as a starting condition to the third and final stage. In the third stage 4 control points are added to the FFD (total of 40 control points). The third stage refines the shape mainly where the shock occurs and after more 28 iterations reached final convergence. In Figure 7 the three adapted FFD frames are presented. The optimization histories are demonstrated in Figure 9. The drag coefficient of the optimized shapes starting from a circle with adaptive FFD is 0.501 counts higher than the optimized shape obtained while starting from RAE-2822. This optimization approach requires 114 iterations. Figure 12 presents a comparison of the final optimized shapes, which are similar to each other. Also presented is a comparison of the pressure coefficient distribution for the

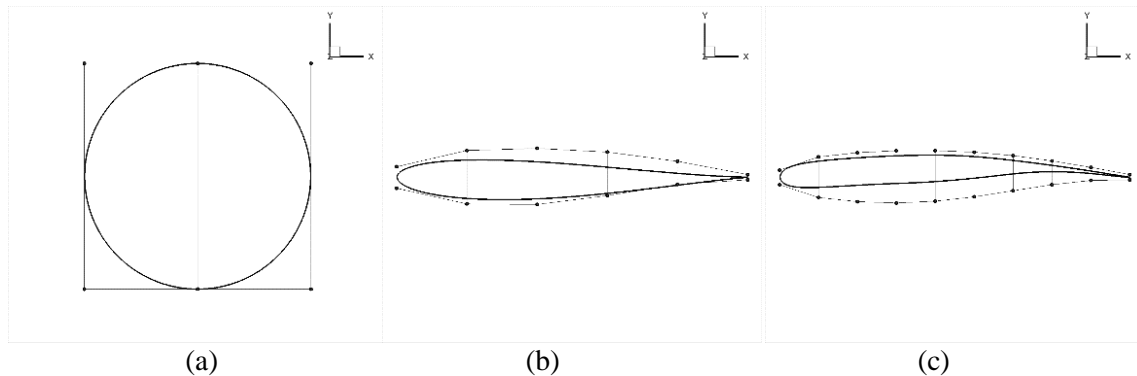


**Figure 7: Adaptive FFD approach for the optimization starting from a circle. a) First stage includes 4 control points. b) Second stage includes 12 control points. c) Third stage includes 20 control points**

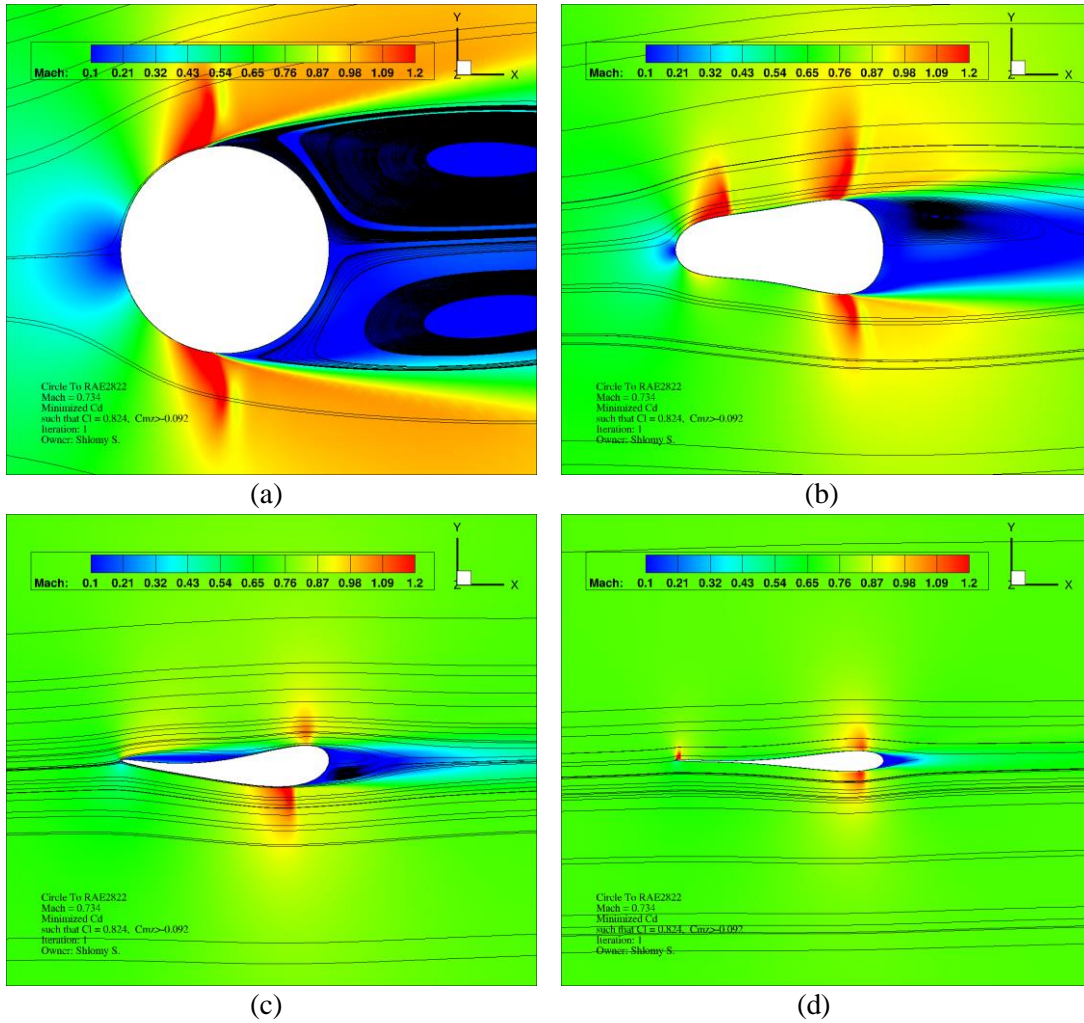


Figure 8: The four initial iterations in the first stage of the optimization starting from a circle.

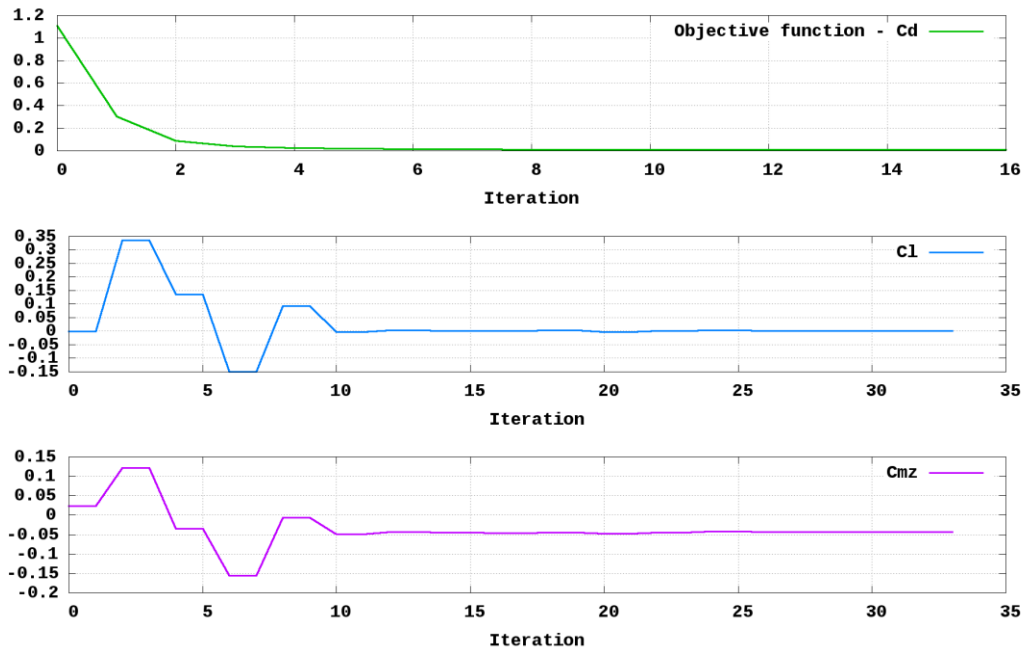


Figure 9: The first stage optimization histories of the optimization starting from a circle

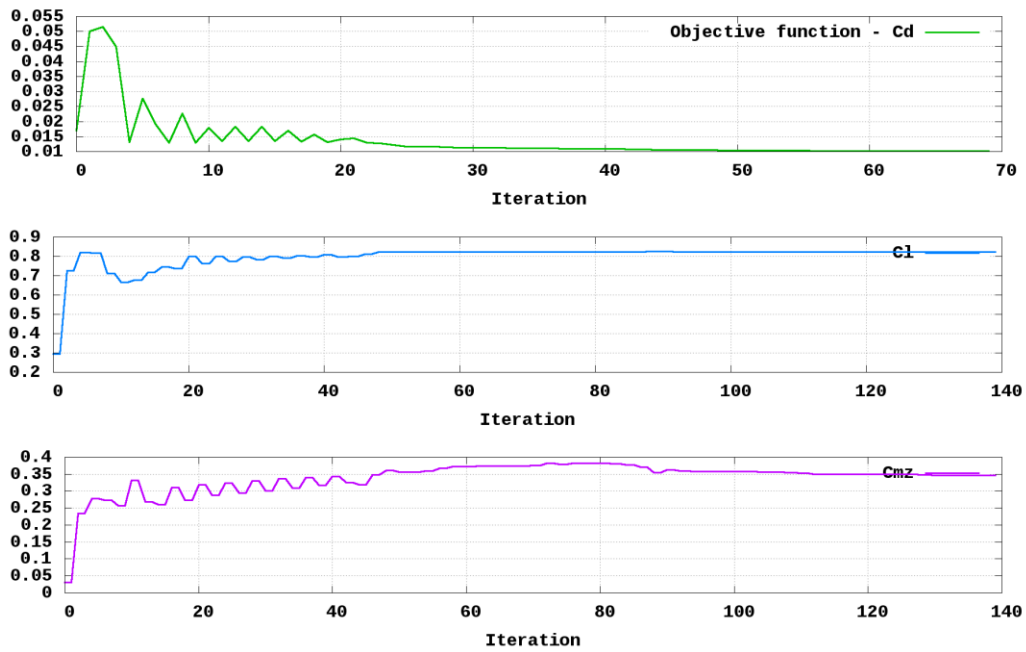


Figure 10: The second stage optimization histories of the optimization starting from a circle

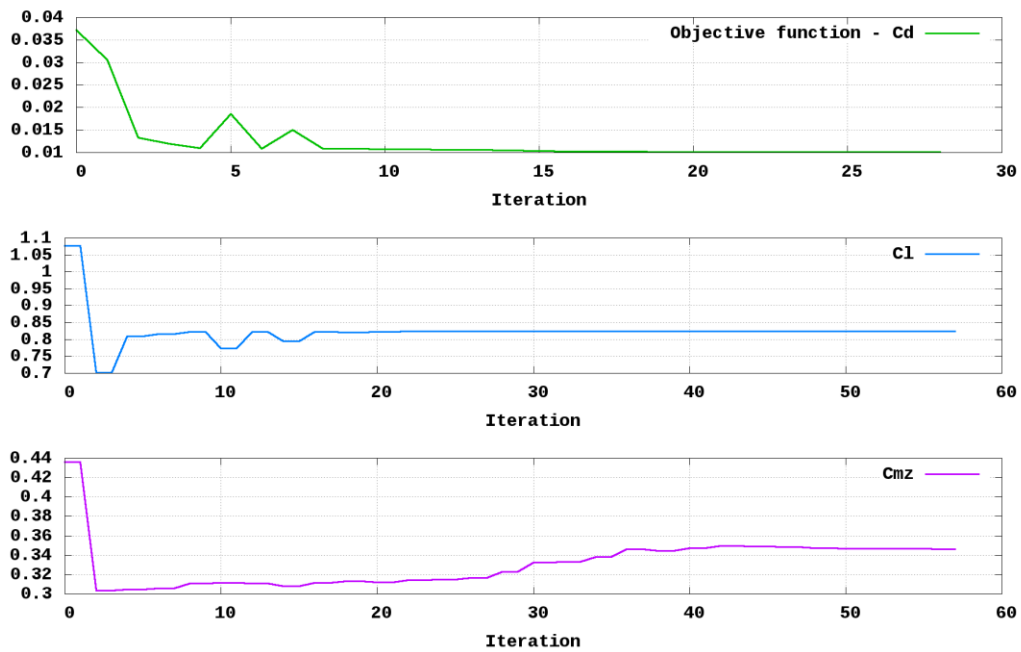
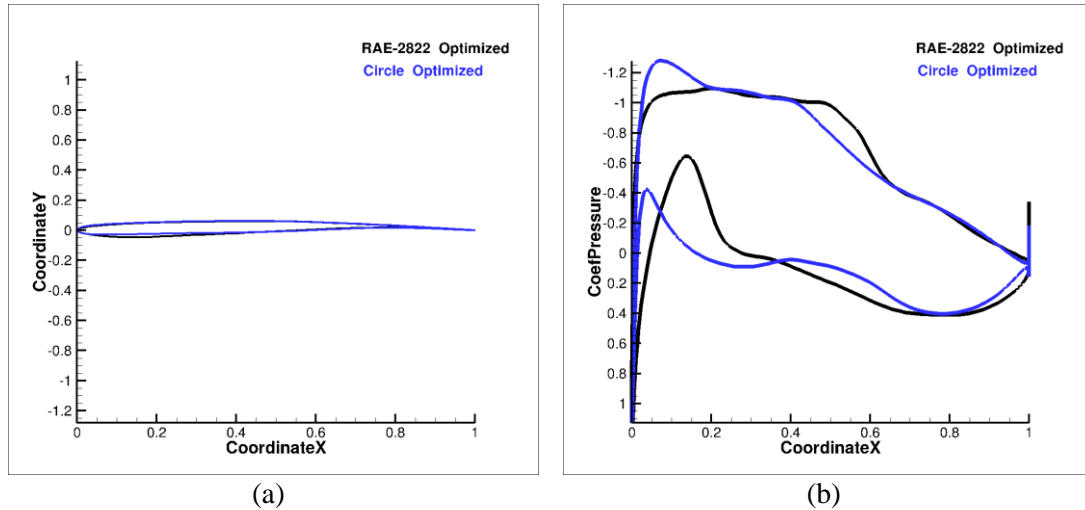


Figure 11: The third stage optimization histories of the optimization starting from a circle



**Figure 12: A comparison between the optimized airfoils. a) Airfoil shapes. b) Pressure coefficient distribution values**

#### IV. Common Research Model (CRM) wing in Turbulent Transonic Flow

##### A. Problem formulation

In this section the drag minimization of the CRM wing is presented. The CRM wing is extracted from the wing-body configuration and was developed for applied CFD validations studies [26]. The sectional shape and twist are optimized in order to minimize the drag coefficient at constant lift coefficient of  $C_l=0.5$ , pitch moment coefficient constraint  $C_{mz} \geq 0.17$ , and at Mach number of 0.85. The Reynolds number, based on the root chord diameter, is  $5 \times 10^6$  (altitude of 12500 m).

Several FFD frames are generated and examined in different approaches and numbers of control points. The main insight from this investigation is that the FFD volume has a dominant importance because it directly relates to how the wing is parametrized. The FFD is fitted very close to the wing surface to allow for better control on the warping procedure. Based on my experience, for faster optimization convergence the control points must be spatially equally set up close to the surface. In Figure 13 the final FFD used for optimization process is presented. The control points used are the y-coordinates normal movements of 192 control points on the FFD frame, 24 chordwise and 8 in the spanwise direction (see

Table 5 and Table 6). The angle of attack is also included in the design variables. The root trailing and leading edges control points are fixed in order to not permit any twist. The trailing edge control points are fixed in order to avoid mesh warping failure, since the tiny thickness in this area. The thickness is controlled by 192 control points in the same order and is set to be 25% greater than the baseline thickness at each control point. The volume is constrained to be greater than or equal to the baseline volume. A list of the control points and constraints are presented in Table 7.

**Table 5: List of design variables used for the optimization of the CRM wing**

Design Variables	Count	Type
shape	192	Y -direction
twist	7	$-10^\circ - 10^\circ$ , Around 30%
Angle of attack	1	$1^\circ - 10^\circ$
<b>Total</b>	<b>200</b>	

**Table 6: Lower and upper bounds for the y-coordinates FFD control points**

	$Z \leq 1.773$	$1.773 < Z \leq 2.72$	$2.72 < Z \leq 3.7$
Lower/Upper bounds	$\pm 0.00375$	$\pm 0.01$	$\pm 0.0005$

**Table 7: List of constraints for the optimization of the CRM wing**

Constraints	Count	Type
Thickness	192	$\geq 0.25 \times t_{baseline}$
Volume	1	$\geq V_{baseline}$
LE, TE control points	32	$<$
Lift Coef., Cl	1	$=$
Pitch moment Coef. Cmz	1	$\geq -0.092$
<b>Total</b>	<b>226</b>	

### B. Initial geometry and grid convergence study

The CRM wing is extracted from the wing-body-tail configuration while replacing the body and tail with a symmetry plane, and the root of the remaining wing is moved to the symmetry plane. The wing geometry is scaled by 275.8 inch, the mean aerodynamic chord, and the origin is located at the root leading edge. Moment's reference point is (1.2007, 0, 0.007669). The reference are for the aerodynamic force coefficients calculations is  $S_{ref} = 3.407$  squared reference units. The initial volume is  $V_{ref} = 0.2617$  cubed reference units. The wing half span is  $L = 3.7$  reference units.

For the grid convergence study three structured hyperbolic volume O-meshes are generated by using pyHyp routine. The initial surface mesh is generated by using the commercial ICEMCFD software. The farfield is located 50L. The coarse grid (level L2) is refined in three directions by a factor of 1.5 and the aerodynamic coefficients and baseline grid size are listed in Table (). The grids generated with clustering cells near the walls which results in a maximum of  $y^+ = 20$ , for the coarsest mesh. Grid convergence study has been made based on the GCI method, for examining the spatial convergence of CFD simulations presented in the book by Roache [24]. The GCI values including the asymptotic range of convergence and an estimation of the aerodynamic coefficient values at zero grid spacing are detailed in Table 8, computed at  $\alpha = 2.4^\circ$ . Based on this study we can say that  $Cd$  is estimated to be  $Cd = 0.02060245$  with an error band of 0.00041%. The grid resolution studies confirmed that the computed aerodynamic coefficients values are grid converged.

It is clearly seen that fine mesh analysis shows that there is some benefit to make an optimization on a finer mesh. However, since all this aerodynamic optimization study is done for an industrial applications, and in industry (compared to academy) there are an inflexible time (and funding) limitations, the subsequent single-point, multi-point and no thickness

reduction problems are conducted using the coarse mesh (Level L5). In this mesh level we can say the error band in predicted Cd value is 0.0875%.

**Table 8: Grid convergence study parameters for the CRM wing**

Grid level	Grid ratio, r	GCI [%]	Cd	Y+
Zero grid spacing			0.02060245	
L0, 4470784 cells	1	-	0.020603	1
L1, 1549184 cells	1.25	0.000411	0.020605	0.5
L2, 1216512 cells	1.42	0.020344	0.020704	0.9
L3, 811008 cells	1.76	0.035433	0.020658	1
L4, 481280 cells	2.10	0.027674	0.020736	2.5
L5, 288768 cells	2.49	0.087445	0.020514	4
L6, 180096 cells	2.91	0.000527	0.020513	6

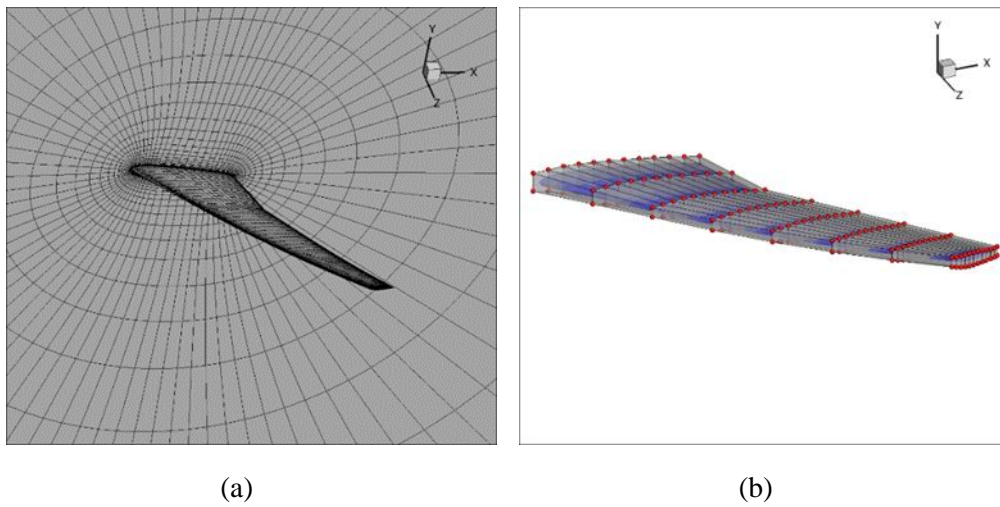


**Figure 13: The computational structured mesh (a) and the FFD mesh (b) of the CRM wing geometry**

### C. Single-point optimization results

For this CRM wing optimization the simulation is started with the DDADI until five order of magnitude reduction in the total residual norm is achieved. Then the solver is switched to ANK for better performance. The relatively selected lower convergence level ( $10^{-5}$ ) for the switch between the solvers improves the robustness of the nonlinear solver, although it comes at the cost of sub-optimal performance for simpler cases. The optimality convergence condition in SLSQP is  $10^{-6}$ .

This optimization problem is challenging to converge mainly because it is sensitive to the mesh warping procedure and the size of the control point's movement values. At the first experience the lower and upper bounds of the y-coordinate control points are defined to move is  $\pm 0.5$  reference units, respectively. This general and straightforward approach results in failures in the warping procedure after few iterations since the large thickness difference along the wing span. Therefore, in order to overcome this limitation, no unified lower and upper thickness bounds are defined, in a way that the wing is divided to eight spanwise sections, with each section consisting of 22 chordwise points (the trailing edge control points are fixed). The lower and upper bounds for each section, from the wing root to the wing tip is detailed in Table 6.

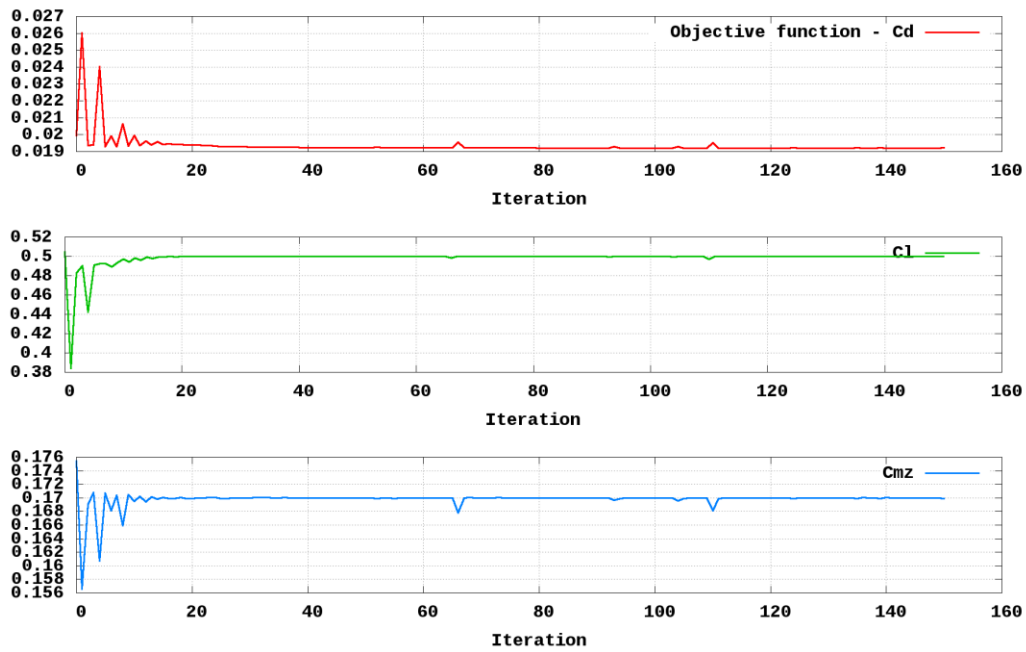


Figure 14: Drag, lift and pitch moment coefficients convergence histories for the single-point optimization of the CRM wing

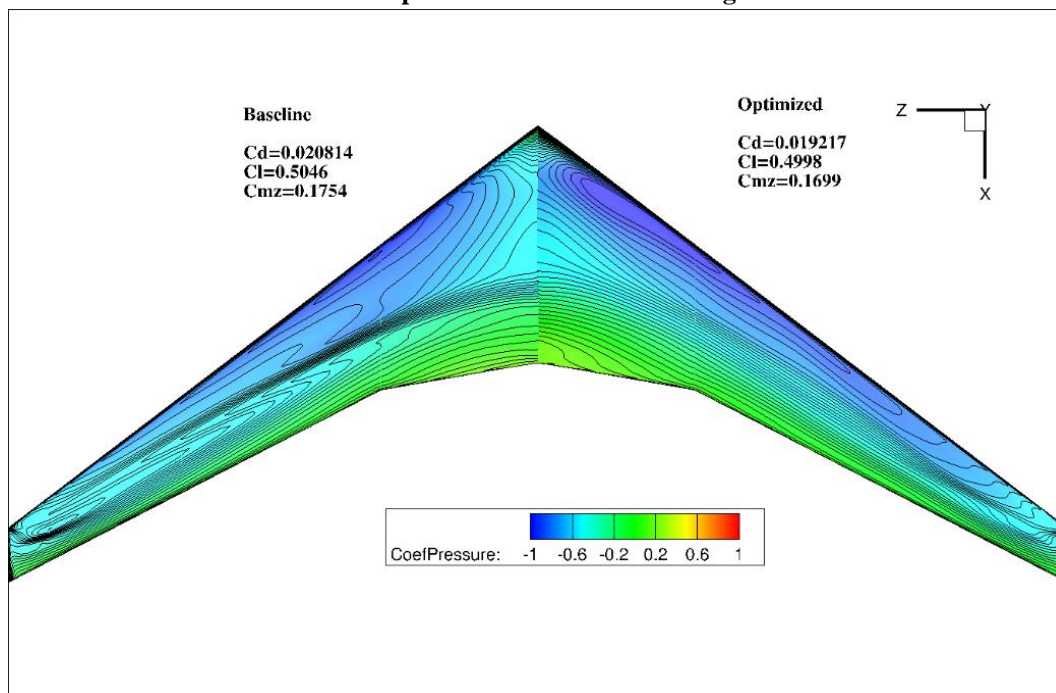
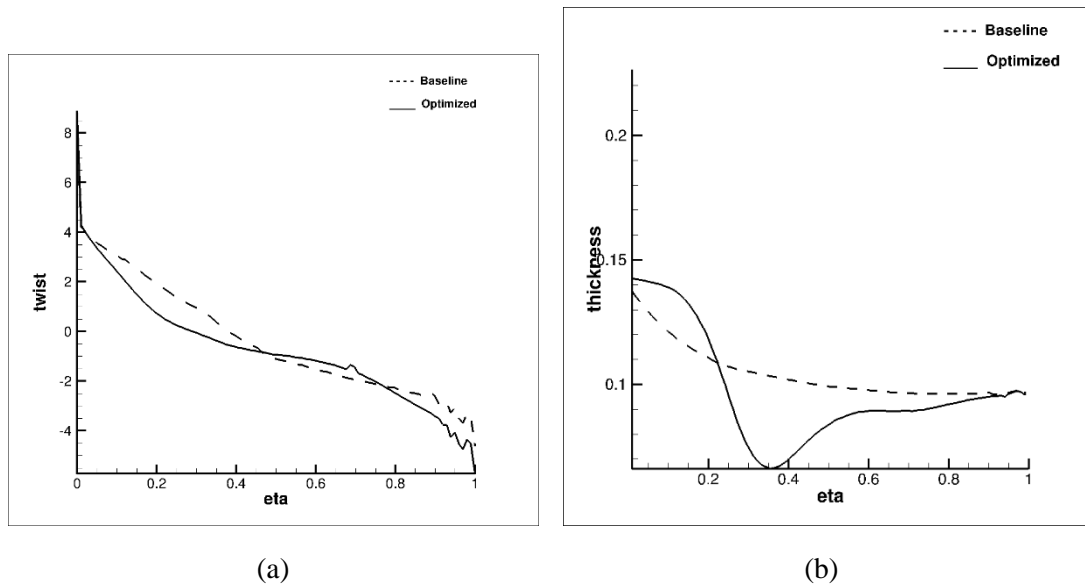


Figure 15: A comparison (mirror view) of the pressure coefficient distribution on the upper surface of the baseline (left) and optimized wing (right). The results obtained with mesh level L5.



**Figure 16; Twist (a) and thickness (b) distribution along the CRM wing span. A comparison between the baseline and optimized geometry.**

The objective function  $C_d$ , the lift and pitch moment coefficients histories are presented in Figure 14. The optimization process decreased the drag coefficient from 208.14 counts to 192.17 counts, namely 16 counts which is a reduction of 7.7%. Taking into account that this wing is designed and tested by experienced engineers, and compared to the impressive work presented by the MDO group [16] which demonstrated a reduction of 8.5% with mesh consists of 28.8 million cells, this is a significant improvement.

The pressure coefficient distribution on the upper surface for both the baseline and optimized wing is shown in Figure 15. One can see the appearance of shock waves generated on the baseline wing, while in the optimized wing these shocks are eliminated. This effect is also demonstrated by the equally spaced pressure contour lines which indicates a shock free solution.

The thickness distribution obtained in the optimized wing is different than the baseline wing (see Figure 16). The optimization algorithm allows thickness reduction of nearly 25%, the lower bound of the thickness constraint. The sectional pressure coefficient is presented in

Figure 17 for four sectional regions scaled from the wing root. Finally, the lift distribution of the optimized wing (see Figure 18) appears to be more elliptical than that of the baseline wing, especially close to the root.

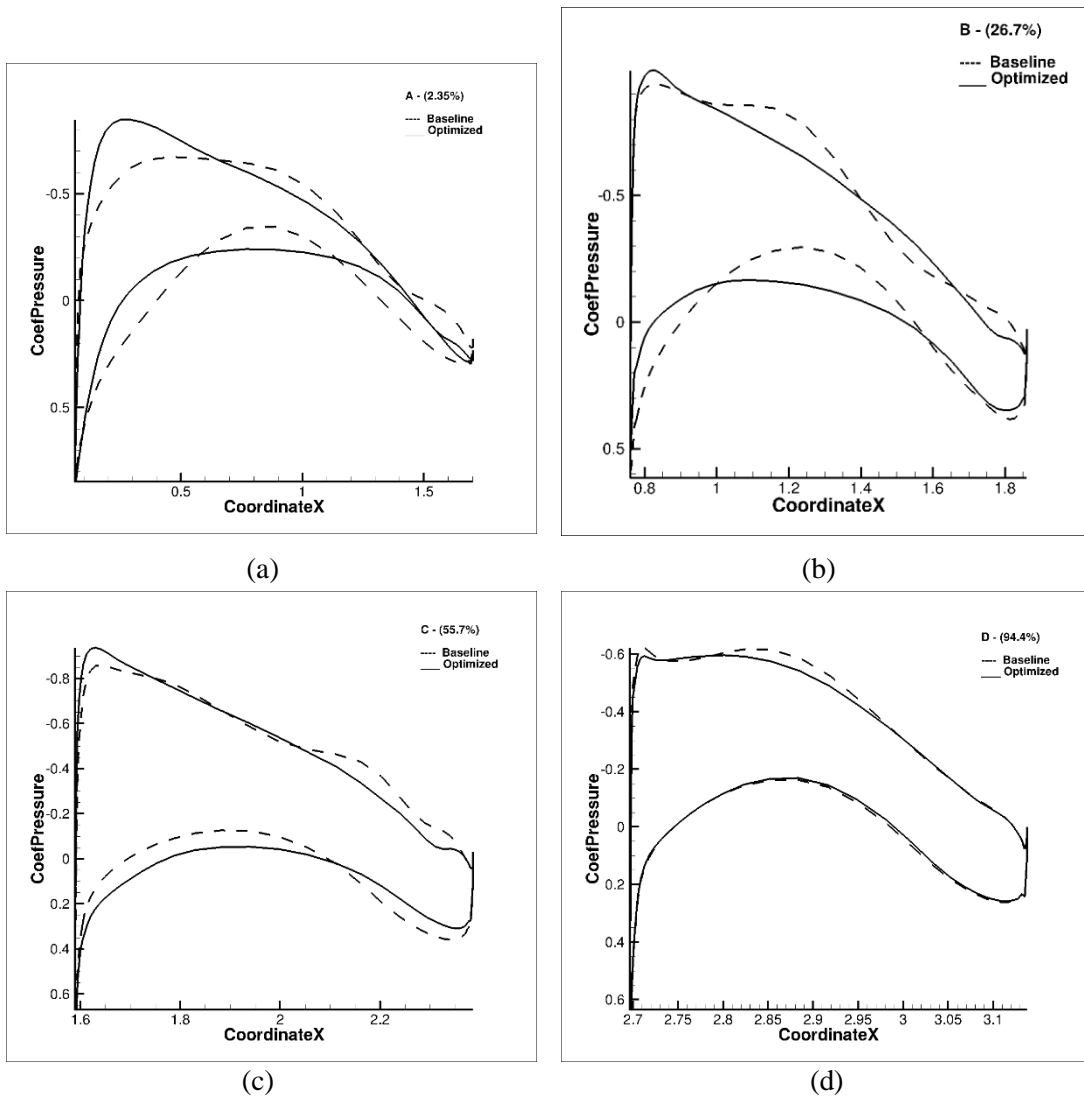


**Figure 17: Sectional Cp distribution at four locations along the CRM wing span, while the numbers 2.35% (a), 26.7% (b), 55.7% (c) and 94.4% (d) represents normalized locations from the wing root.**

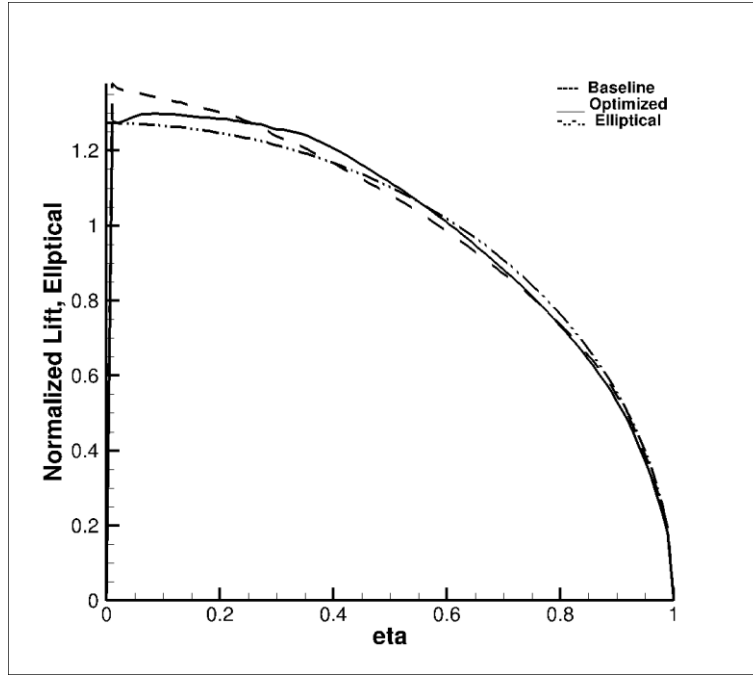


**Figure 18: Baseline, optimized and elliptical normalized lift distribution along the CRM wing span**

**Table 9: Results for the CRM wing single-point optimization**

Mesh level	Mesh size	Baseline Cd	Optimized Cd	Delta Cd (counts)	Cl	Y+	Optimized Cmz	Optimized alpha
L00	1216512	0.020704	0.019217	14.9	0.4998	0.9	0.1699	<b>2.91</b>
L11	811008	0.020658	0.019043	16.1	0.4999	1	0.1699	<b>3.00</b>
L22	481280	0.020736	0.019403	13.3	0.5000	1	0.1700	<b>3.24</b>
L33	288768	0.020514	0.019363	11.5	0.5000	4	0.1699	<b>3.39</b>
L44	288768	0.018937	0.017840	10.9	0.4999	10	0.1699	<b>2.88</b>

Another grid convergence study is conducted in order to check if the correct design trends are captured. For this purpose the single point optimization process is repeated five times with different mesh resolutions and the results are summarized in Table 9. The difference between the Richardson's extrapolation (zero grid spacing, presented in Table 8) and the drag coefficient for Level L00 is within 1 drag count. In addition, the difference between the baseline and optimized drag coefficients is approximately 14 counts on average while reaching an asymptotic level of 16 counts. The desired drag resolution of 1 count is achieved between the two finest levels, including the lift and pitch moment constraints. According to this grid convergence study and the fact the main focus of this analysis is to establish an aerodynamic optimization capability in a way that would fit the time and resources limitations exist in industrial applications, the remaining optimization cases are computed by using the coarser mesh L33.

#### **D. Single-point optimization without thickness reduction**

As already mentioned, the CRM optimization case is challenging to converge mainly because of the varying thickness which becomes 30% lower at the wing tip compared to the wing root thickness. This mesh warping method is strongly affected by this constraint and it results in a

very tight values that define the control point's movements. It is clearly shown that the baseline wing has two shocks on upper surface, one at the middle and smaller one close to the wing tip. Since the main challenge of this problem is to minimize the wave drag generated by shock waves while satisfying the minimum thickness constraint, it results in a much lower thickness values at the tip, and not sure that the optimized wing can withstand structural constraints, which are not taken into consideration in this optimization problem.

Another point of view on this issue is that a wing with a low outboard thickness would probably weights much higher, since the wing structural strengthening is unavoidable. This is what motivates the following optimization, reducing the wave drag without reducing the wing thickness at all. All other constraints remains the same as is detailed in Table 7.

The optimization histories are presented in Figure 19. The optimization procedure reduced the drag coefficient from 205 counts to 195 counts, nearly 3 counts higher than the optimized wing that allowed 25% of the baseline thickness. This optimization process is faster, and it takes nearly 150 iterations compared to the optimization described in previous chapter.

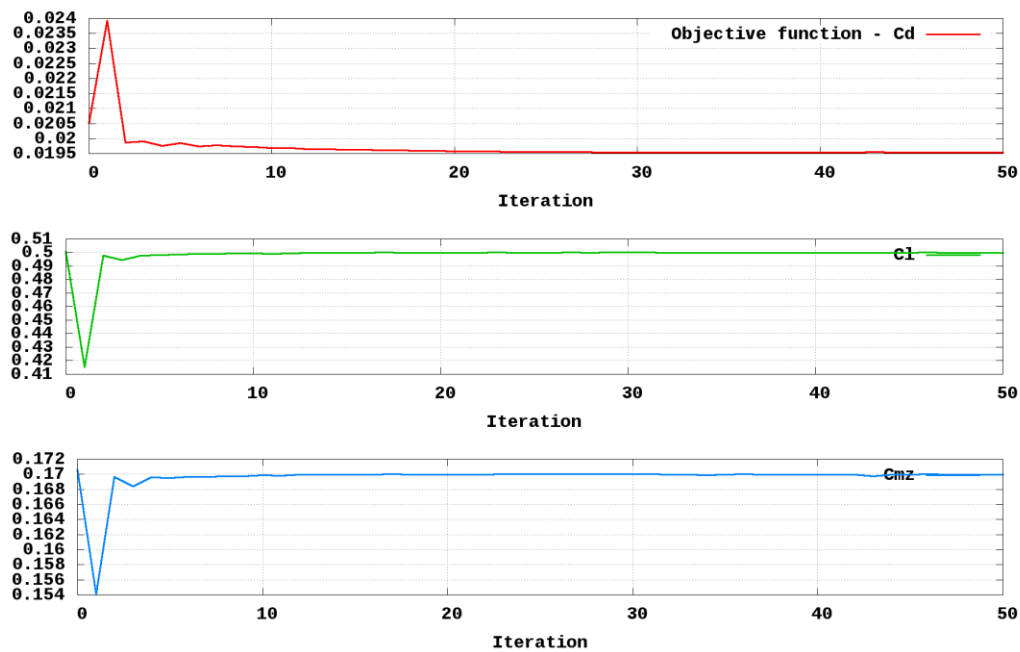


**Figure 19: Drag, lift and pitch moment coefficients histories for the CRM wing optimization with no thickness reduction**

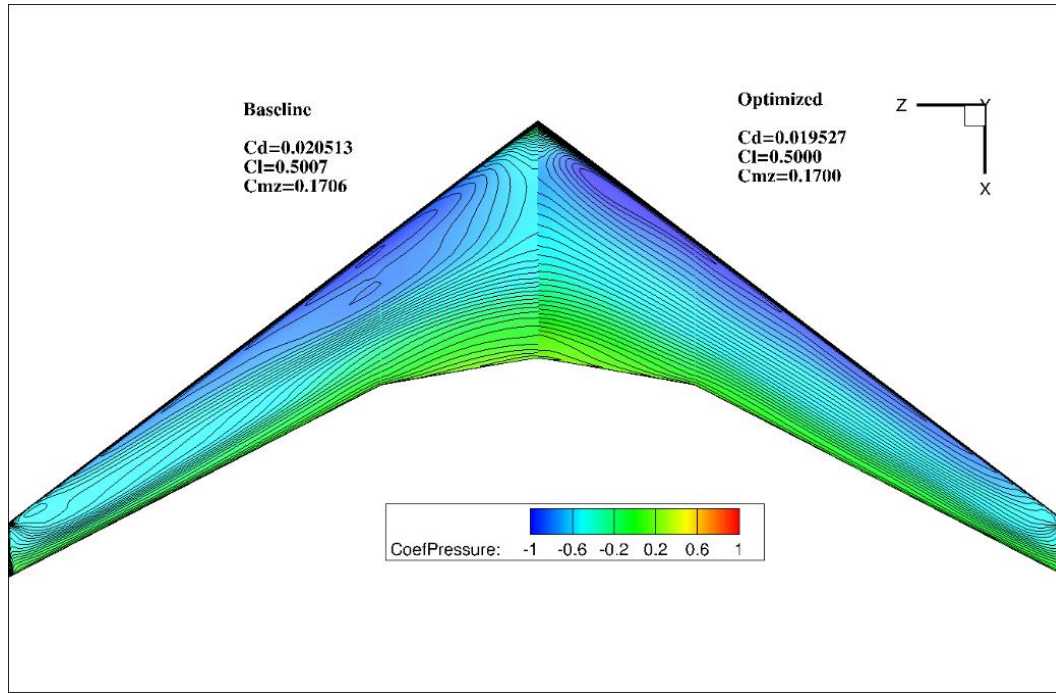


**Figure 20: A comparison (mirror view) of the pressure coefficient distribution on the upper surface of the baseline (left) and optimized wing (right) with no thickness reduction. The results obtained with mesh level L2.**

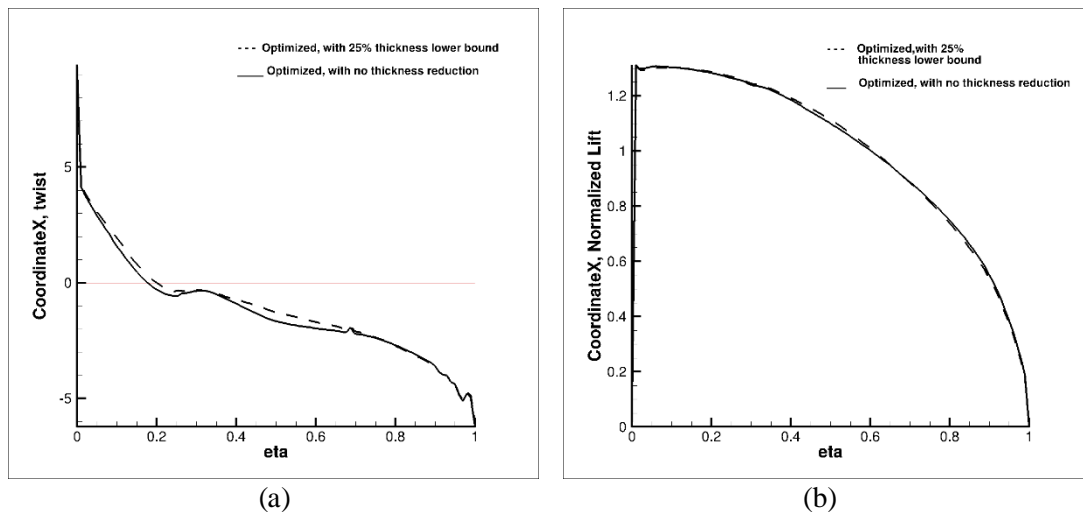


**Figure 21: Twist (a) and normalized lift distribution (b) along the CRM wing span, optimized with no thickness reduction.**

### E. Five-points aerodynamic shape optimization

This section follows the multi-point optimization conditions studied in [10]. The problem includes five-points with variables  $Cl$  and variables Mach number. The  $Cl$  and Mach number variation is done by perturbing the nominal values by 10%. The operating points are summarized as follows: C1:  $Cl = 0.5, M = 0.85$ , C2:  $Cl = 0.55, M = 0.85$ , C3:  $Cl = 0.45, M = 0.85$ , C4:  $Cl = 0.5, M = 0.84$ , C5:  $Cl = 0.5, M = 0.86$ . The objective function is the averaged drag coefficient. The pitching moment coefficient is only satisfied at the nominal operating point (C1).

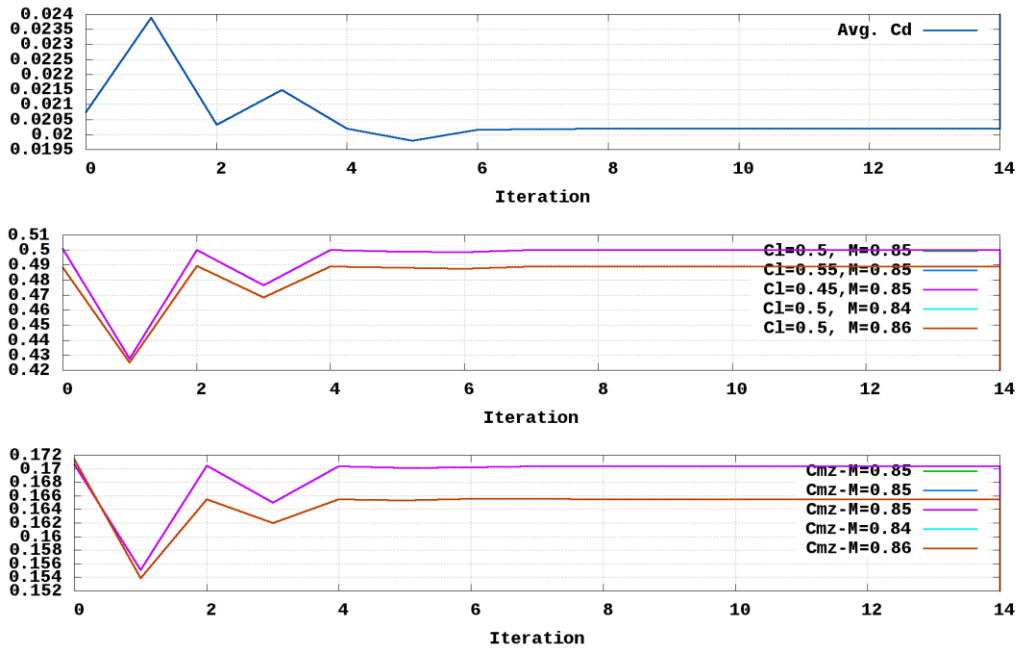


**Figure 22: Average drag, lift and pitch moment coefficients histories for the five-points CRM wing optimization**

The optimization histories are presented in Figure 22. The five-point optimizations converged successfully after only 14 design iterations and the lift and pitch moment constraints are obtained. The pressure coefficient distribution on the upper surface for the optimized five-point case compared to the single-point case, is presented in Figure 23. The sectional pressure plots computed at the nominal condition (C1) are displayed in Figure 24. The five-point case, compared to the single-point optimization shows poorer performance at the nominal flight conditions. The drag coefficient at the nominal flight conditions (C1) is reduced from 207.5 counts to 201.94 counts, 8.3 counts higher than the single-point case, while the averaged drag coefficient is reduced by 5.6 counts. The optimized wing contains a weak shock wave in the middle of the wing, which exists in all the operating conditions.

The thickness distribution in the nominal conditions ( $M=0.8$ ) obtained in the five-point optimized wing is different than the single-point case (see Figure 25). The optimization algorithm allow thickness reduction of nearly 25%, the lower bound of the thickness constraint. The resulted five-point optimized wing is less twisted and thinner than the single-point optimized wing.

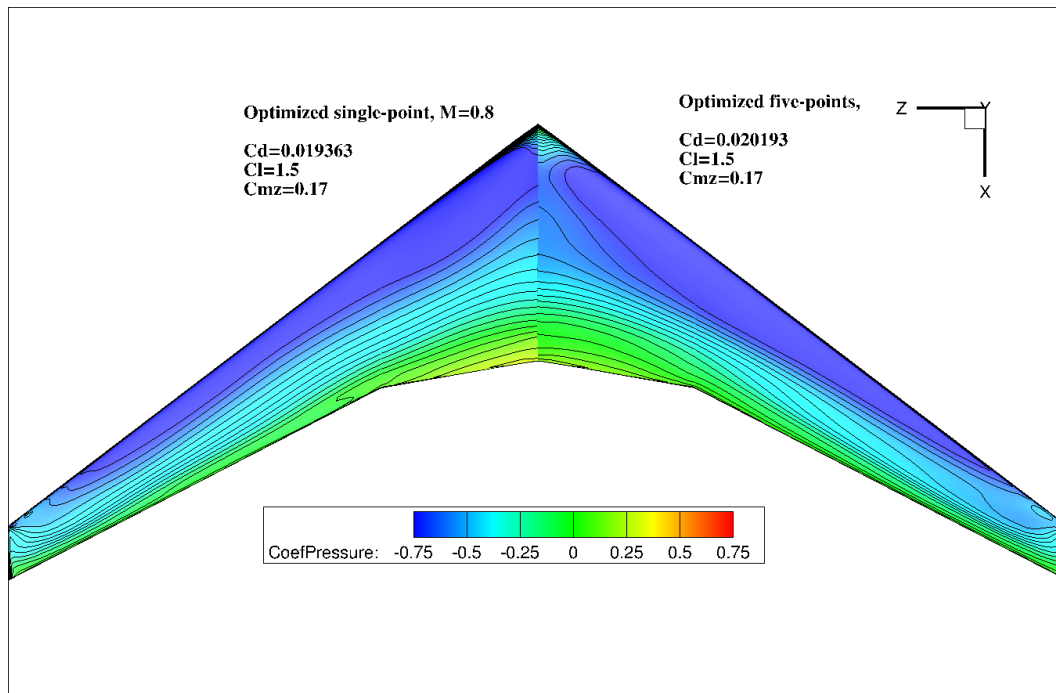
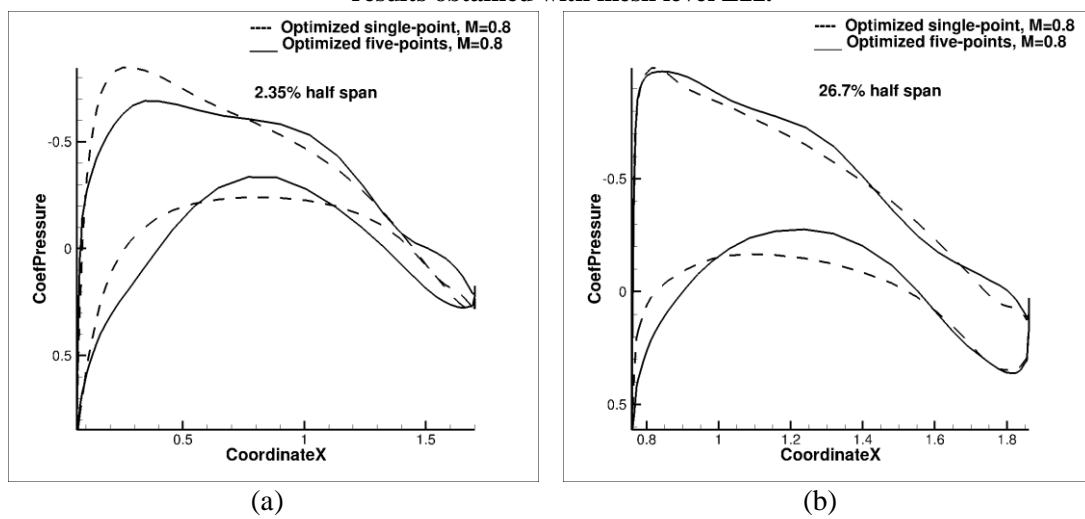


Figure 23: A comparison (mirror view) of the pressure coefficient distribution on the upper surface of the single-point optimized wing (left) and the five-point optimized wing (right). The results obtained with mesh level L22.



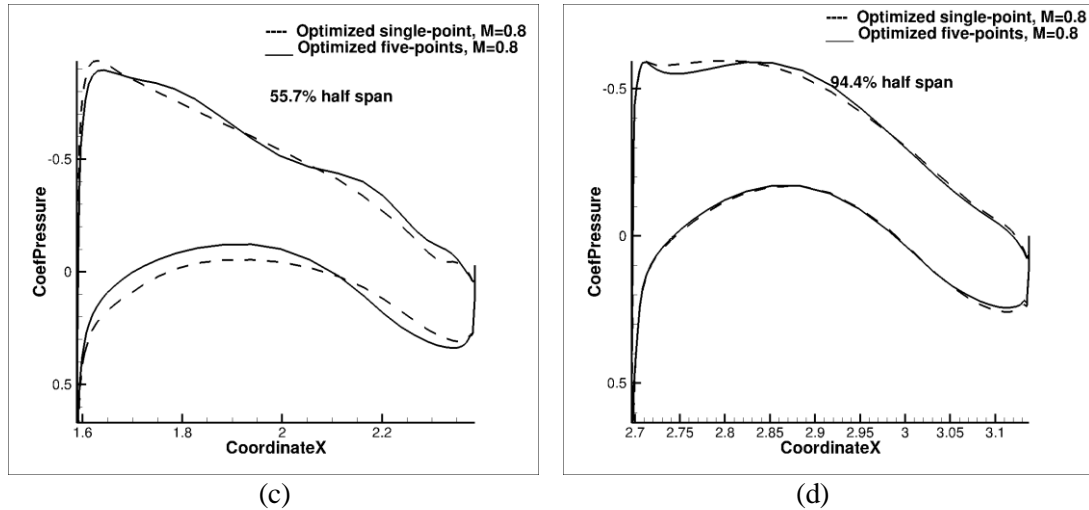


Figure 24: Sectional Cp distribution at four locations along the CRM wing span, while the numbers 2.35% (a), 26.7% (b), 55.7% (c) and 94.4% (d) represents normalized locations from the wing root.

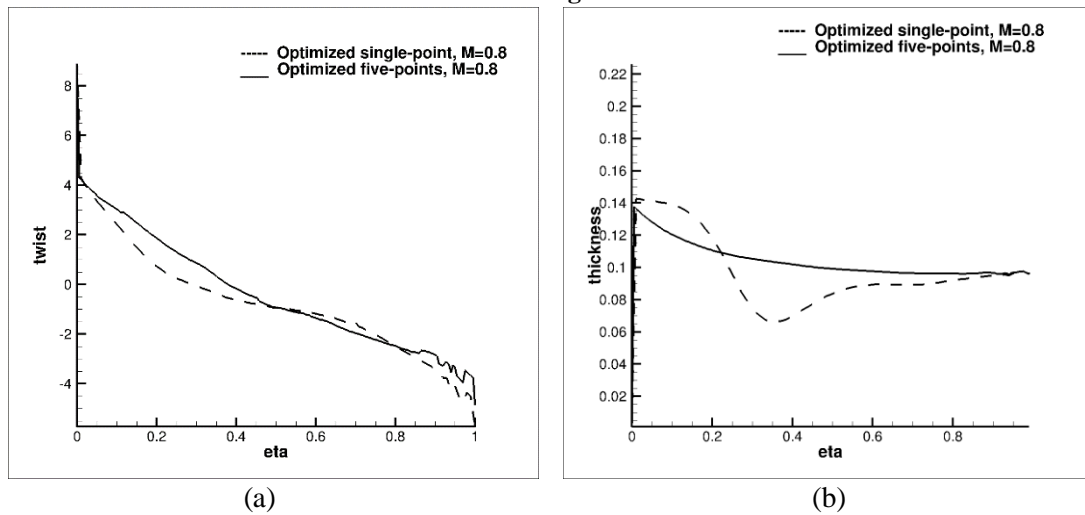


Figure 25: Twist (a) and normalized lift distribution (b) along the five-points optimized CRM wing span. The results are for the nominal flow conditions ( $M=0.8$ ).

## V. Conclusions

This study presents a modest experience to construct an aerodynamic optimization capabilities based on the gradient based algorithms together with an adjoint method that computes the required gradients efficiently, developed in the University of Michigan MDO Lab. The main motivation for this research is analyzing the sensitivity and robustness of the flow solver, mesh warping method and the optimization algorithm to reduced sized problems, in a way that would fit the time and resources limitations exist in industrial applications. The effectiveness of the optimization process is demonstrated by benchmarking the ADODG RAE-2822 and CRM wing optimization cases. For both ADODG cases we obtain well converged results which are comparable to the results from previous work.

For the RAE-2822 case, a drag coefficient reduction of 971 Counts (49.2%) was obtained within 100 design iterations. The main challenge of this problem involves minimizing the wave drag while satisfying the thickness and lift constraints. The shock wave appeared in the baseline configuration is eliminated in the optimized shape and the thickness is reduced by nearly 15% compared to the initial value.

Also in this case, the robustness of the flow solver and mesh warping algorithm is demonstrated by starting the optimization process from a circle geometry (and not airfoil RAE-2822). In spite of the fact that this preferred starting condition might not be of interest for industrial applications, it definitely examines the robustness of the numerical method as well as the FFD parametrization method. The optimized shapes starting from RAE-2822 and circle are similar to each other except for minor differences. The drag coefficient of optimized shapes starting from a circle and from the RAE-2822 differ by 0.501 counts only.

For the CRM wing case, the single-point optimization on the coarse mesh with 192 FFD control points reduces the drag coefficient by 16 counts (7.7%). The no thickness reduction case results in additional five counts compared to the optimized with that allowed 25% of the baseline thickness. The five-point optimization gives higher drag coefficient at the nominal condition compared to the single-point optimization, and also in this case a significant shape changes and improved performance are achieved.

- [1] J. E. V. Peter and R. P. Dwight, "Numerical sensitivity analysis for aerodynamic optimization: A survey of approaches," *Computers and Fluids*, pp. 373-391, 2010.
- [2] J. R. R. A. Martins and J. T. Hwang, "Review and unification of methods for computing derivatives of multidisciplinary computational models," *AIAA*, pp. 2582-2599, 2013.
- [3] J. R. R. A. Martins, P. Sturdza and J. J. Alonso, "The complex-step derivative approximation," *ACM Transactions on Mathematical Software*, pp. 245-262, 2003.
- [4] O. Pironneau, "On optimum design in fluid mechanics," *Journal of Fluid Mechanics*, vol. 64, pp. 97-110, 1974.
- [5] A. Jameson, "Aerodynamic design via control theory," *Journal of scientific computing*, vol. 3, pp. 233-260, 1988.
- [6] A. Jameson, "Computational algorithms for aerodynamic analysis and design," *Applied Numerical Mathematics*, pp. 383-422, 1993.
- [7] D. A. Anderson, J. C. Tannehill and R. H. Pletcher, *Computational Fluid Mechanics and Heat Transfer*, New York: McGraw-Hill Book Company, 1984.
- [8] L. C. L and H. R. J, "Solving Least Squares Problems," *Classics in Applied Mathematics*, SIAM, p. Volume 15, 1987.
- [9] E. J. Nielsen and W. K. Anderson, "Aerodynamic design optimization on unstructured meshes using the Navier{Stokes equations,," *AIAA*, pp. 1411-1419, 1999.
- [10] Z. L. G. K. W. K. J. R. R. A. M. S. Chen, "Aerodynamic shape optimization of the Common Research Model wing-body-tail con," *Journal of aircraft* 53, pp. 276-293, 2016.
- [11] Z. L. Z. X. J. R. R. A. M. Y. Yu, "On the influence of optimization algorithm and starting design on wing aerodynamic shape optimization,," *Aerospace Science and Technology* 75 , pp. 183-199, 2018.
- [12] C. A. Mader, "ADjoint: An Approach for the Rapid Development of Discrete Adjoint Solvers," *AIAA Journal*, vol. 46, 2008.
- [13] X. He, J. Li, C. A, Mader, A. Yildirim and J. R. R. A. Martins, "Robust aerodynamic shape optimization-from a circle to an airfoil," *Aerospace Science and Technology*, pp. 48-61, 2019.

- [14] C. Song, L. Zhoujie, K. W. K. Gaetan and R. R. A. M. Joaquim, "Aerodynamic Shape Optimization of the Common Research Model Wing-Body-Tail Configuration," in *AIAA SciTech Forum*, Florida, 2015.
- [15] J. R. R. A. Martins, "Multidisciplinary Design Optimization of Aircraft Configurations," Von Karman Institute for Fluid Dynamics, Belgium, 2016.
- [16] G. K. K. a. J. R. R. A. M. Zhoujie Lyu, "Aerodynamic Shape Optimization Investigations of the Common Research Model Wing Benchmark," *AIAA Journal*, 2014.
- [17] L. Christopher and e. al, "Aerodynamic Shape Optimization of Benchmark Problems Using Jetstream," *American Institute of Aeronautics and Astronautics*, 2018.
- [18] J. R. R. A. Martins, K. W. K. Gaetan and T. Brooks, "Multidisciplinary Design Optimization of Aircraft Configurations - part2: High fidelity aerostructural optimization," in *Lecture series, Von Karman Institute for Fluid Dynamics*, Sint Genesius Rode, Belgium, 2016.
- [19] E. K. G. S. J. a. A. J. van der Weide, "Unsteady Turbomachinery Computations Using Massively Parallel Platforms," in *44th AIAA Aerospace Sciences Meeting and Exhibit*, 2006.
- [20] A. S. W. a. T. E. Jameson, "Numerical Solution of the Euler equations by Finite Volume Methods Using Runge Kutta Stepping Schemes," in *14th AIAA, Fluid and Plasma Dynamics Conference*, 1981.
- [21] G. K. W. Kenway, G. J. Kennedy and J. R. R. A. Martines, "A CAD-free Approach to High Fidelity Aerostructural Optimization," in *13th AIAA/ISSMO Multidisciplinary Analysis Optimization Conference*, Fort Worth, 2010.
- [22] R. E. Perez, P. W. Jansen and J. R. R. A. Martins, "A Python-based object-oriented framework for nonlinear constrained optimization, Structural and Multidisciplinary Optimization," 2012.
- [23] D. Kraft, "A software package for sequential quadratic programming," DLR German Aerospace Center, 1988.
- [24] P. J. Roache, K. Ghia and F. White, "Editorial Policy Statement on the Control of Numerical accuracy," *ASME Journal of Fluids Engineering*, p. 2, 1986.
- [25] P. H. Cook, M. A. McDonald and M. C. P. Firmin, "\Aerofoil RAE 2822 - Pressure Distributions, and Boundary Layer and Wake Measurements," Experimental Data Base for Computer Program Assessment, AGARD Advisory Report, No 138, 1979.
- [26] J. D. M. R. M. a. W. R. Vassberg, "Development of a Common Research Model for Applied CFD Validation Studies," *American Institute of Aeronautics and Astronautics*, 2008.
- [27] A. Jameson, "Aerodynamic design via control theory," *Journal of Scientific computing*, pp. 233-260, 1988.
- [28] W. K. Anderson and V. Venkatakrishnan, "Aerodynamic design optimization on unstructured grids with a continuous adjoint formulation,," *Computers and Fluids*, pp. 443-480, 1999.
- [29] "<https://github.com/mdolab/MACH-Aero>," University of Michigan, 2019. [Online].